Eighth Australasian Fluid Mechanics
Conference, University of Newcastle,
N.S.W., 28 November/2 December 1983.

DEVELOPMENT OF LARGE DISTURBANCES INTO TURBULENT SPOTS

S.I. CHENG, MA AND S. ROY

DEPARTMENT OF MECHANICAL ENGINEERING

PRINCETON UNIVERSITY, PRINCETON, NJ 08544 U.S.A.

SUMMARY Experimental observations and mathematical theory suggest the wave nature of shear flow turbulence with discrete propagating fronts. We report how a physical mechanism of wave generation by vorticity transport helps to eliminate numerical turbulence in the computational simulation of the development of disturbances into turbulent spots. The deterministic view of shear flow turbulence as chaotic solution with coalesced wave fronts is thus constructively demonstrated.

INTRODUCTION

The intermittent nature of turbulent wake behind a cylinder was reported by Townsend (1947). The possibility of a double layer structure with a nearly isotropic turbulent core, sweeping and growing in the surrounding laminar flow, was suggested. An individual growing turbulent spot, hugging onto a solid plate surface while propagating downstream was reported by Emmons (1951). A double layer structure was also proposed with a "fully turbulent" anisotropic flow in the spot. Interaction of spots was said to be "passive" that their overlapped region is not significantly different. With many such spots generated upstream, these growing spots will soon cover the downstream region as a fully turbulent flow with its outer edge consisting of the remnants of the aggregated turbulent spots. Intermittency and organized structures at various scales have since been generally observed in both free and wall turbulence (Hinze 1975, Cantwell 1981). They are recognized but little understood.

A double layer structure appears simplistic. On the other hand, a multi-layer structure with a hierarchy of entities having discrete boundaries propagating into neighbouring states is confusing and disturbing. Thus it is often more desirable to study some ensemble average in a set of experiments. The discrete feature of large structures and global vortical motion will then stand out. For instance, a diffused horseshoe vortex appears in a turbulent spot. The aggregation of many turbulent spots of varied sizes will display Theodorsen's picture (1955) of a turbulent boundary layer as some chaotic superposition of horseshoe vortices. More recently Perry et al (1980) proposed to superpose strings of Λ vortices to reproduce many mean features of wall turbulence. Thus turbulence as a multi-layer structure in terms of a hierarchy of large and small entities with discrete propagating boundaries appears to display many features of experimental observations.

Ruelle and Takens (1971) suggested turbulence as represented by chaotic solutions of bifurcating nonlinear systems. Fluid turbulence is deterministic as the chaotic solution of initial boundary value problems of the Navier-Stokes (N-S) system at sufficiently large Reynolds numbers. The successive bifurcation fronts in $(\underline{x},t)$ are discrete, finite propagating waves in physical space $\underline{x}$, giving rise to the multi-layer structure. Thus, the solution of initial value problems of the N-S system is expected to present major features of turbulent shear flows. Many computational simulations have generated chaotic fields but failed to show the discrete features of shear flow turbulence. With the computed velocity fields not solenoidal they are not physical, often called numerical turbulence.

Turbulence has traditionally been considered as a diffusive phenomenon in a convective field, represented by vorticity transport equations, and/or a hierarchy of transport equations of velocity moments of N-S. Much effort has been dedicated to the solution of these transport equations with some closure postulate. Energy cascading down to dissipation scale eddies is essential to the statistical theory(ies) and has guided the ad hoc turbulence modeling, global or subgrid, for the solution of practical problems. The discrete nature of turbulence is either overlooked or dismissed as a purely transitional phenomenon. The failure of computational simulation is supposed to be due to the lack of sufficiently refined computational resolution. A convergent approximation at sufficiently small Δx is presumed to be free of numerical turbulence.

A chaotic solution is, however, sensitive to data perturbation and not well set for convergent approximation as $\Delta x \to 0$. We can only compute at coarse meshes for adequate asymptotic approximations to capture the global features of the turbulent field. Hence numerical turbulence must be distinguished and removed. The asymptotic nature of coarse mesh computation and a criterion to identify the best approximation were demonstrated for the steady state solution of the N-S (Cheng, 1982). The same should be true for time dependent solutions. The global asymptotic features of the first few bifurcations should not be adversely affected by the small scale later bifurcations. The stability requirement for computing unstable flows is less demanding than that of the steady state problem. The origin of the violent numerical turbulence is likely not numerical. All these contradict the expectations of statistical theory. A successful computational simulation at coarse mesh of the global wave features of shear flow turbulence will contribute much to the resolution of these issues. To this end the physical wave mechanism must first be identified and a method of avoiding numerical turbulence devised.

A physical mechanism of wave generation by vorticity transport in a turbulent field was proposed (Cheng, 1983). A velocity disturbance in a flow field must be accompanied by suitable pressure disturbances. The first part is to provide the spatial gradient for generating the velocity disturbance locally according to Newton's Law. The second part is a harmonic pressure field to maintain a solenoidal velocity field (and vorticity). They are the eigen solutions of the Poisson equations for pressure under nontrivial boundary conditions. The spectral content of these eigen solutions is determined by $\nabla \underline{q} = 0$ for all $\underline{x},t$. They may be interpreted dynamically as the impulsive force pairs required to eliminate the residual divergences of both physical and computational origin (Lamb, 1932). These impulses generate waves propagating throughout the field to alter the velocity and pressure, far and

near, to establish the smooth pressure disturbances associated with the initial velocity disturbance. A smooth, quasi-steady asymptotic state may soon be reached, consistent with the Biot-Savart Law. Under other conditions, local coalescence of converging waves lead to discrete fronts of turbulent quantities, propagating in $(\bar{x},t)$ with different group velocities, and riding over one another. They represent local solution bifurcations. A section view will look like the ocean surface with waves, wavelets and breaks and occasionally local storms or other catastrophic events. When the eigen solutions of the pressure field and their associated velocity field have been calculated, the appropriate spectrum of these eigen solutions can be determined so that the synthesized velocity field is solenoidal. This is clearly a tedious and inaccurate computational proposition.

COMPUTATIONAL SOLUTION OF SPOT DEVELOPMENT

We take advantage of the large signal speed to avoid calculating the eigen states and their spectral content. The process of wave relaxation to a solenoidal field is too fast for any viscous action to respond so that the induced field can be derived from some potential function. Thus any non-physical states of vorticity $\bar{\zeta}$ and velocity $\bar{q}_r$ with residual divergences can be restored to the physical solenoidal states $\bar{\omega}$ and $\bar{q}$ by the addition of $\nabla\psi$ and $\nabla\phi$ respectively.

i.e.
$$\bar{\omega} = \bar{\zeta} + \nabla\psi \tag{1}$$

$$\bar{q} = \bar{q}_r + \nabla\phi \tag{2}$$

with
$$\nabla^2\psi = -\text{div}\ \bar{\zeta} \tag{3}$$

$$\nabla^2\phi = -\text{div}\ \bar{q}_r \tag{4}$$

Then the computation to advance a physical state $\bar{q}^n(\bar{x},t)$, $\bar{\omega}^n(x,t)$ and $p^n(x,t)$ at $t = n\Delta t$ to the next time step $t = (n+1)\Delta t$ will consist of the following:
(a) Vorticity loop to obtain a solenoidal $\bar{\omega}^{n+1}$ for a given solenoidal $\bar{q}^n$, or $\bar{q}^{n+\frac{1}{2}}$ as some average convective velocity.
(b) Velocity loop to obtain a solenoidal $\bar{q}^{n+1}$ for the latest available $\bar{\omega}^{n+1}$.
(c) Quasi-linearization loop to correct the average convective velocity $\bar{q}^{n+\frac{1}{2}}$.
(d) Calculate $p^{n+1}(x,t)$ from the converged, solenoidal velocity and vorticity fields $\bar{q}^{n+1}$ and $\bar{\omega}^{n+1}$.

The vorticity transport equation

$$\frac{\partial\bar{\omega}}{\partial t} = \nabla\times(\bar{q}\times\bar{\omega}) + \frac{1}{Re}\nabla^2\bar{\omega} \tag{5}$$

with an approximate boundary formulation in terms of the latest available data is used to advance $\bar{\omega}^n$ to $\bar{\zeta}^{(n,1)}$. Equation (3) is then solved with the Neumann condition $\partial\psi/\partial\nu = 0$ on all boundaries with normal $\bar{\nu}$ so as to avoid disturbing the nonslip solid surface condition: $\bar{\nu}\cdot\bar{\omega} = 0$. The new solenoidal iterate $\bar{\omega}^{(n,1)}$ is then obtained from (1) to repeat the loop with (5). This vorticity loop terminates when $\|\bar{\omega}^{(n,s+1)} - \bar{\omega}^{(n,s)}\|$ is less than some predetermined value.

The uncoupled Poisson equation

$$\nabla^2\bar{q} = -\nabla\times\bar{\omega} \tag{6}$$

is solved in preference to the coupled system $\nabla\times\bar{q} = \bar{\omega}$ with the physical boundary condition of $\bar{q}$ to obtain the nonsolenoidal $\bar{q}_r^{(n,1)}$. Equation (4) is then solved with $\partial\phi/\partial\nu = 0$ on all boundaries. The solenoidal velocity iterate $\bar{q}^{(n,1)}$ is then obtained from (2) and the boundary values of $\bar{q}_r$ corrected before equations (6) are solved in the next iterative cycle. The velocity loop terminates with sufficient small $\|\bar{q}^{(n,s+1)} - \bar{q}^{(n,s)}\|$.

The quasi-linearization loop is initiated by evaluating the average convective velocity $\bar{q}^{n+\frac{1}{2}}$ from the latest available iterate of $\bar{q}^{n+1}$ according to some chosen format. Repeat the vorticity loop (a) and the velocity loop (b) until satisfactory convergence is obtained. Finally the pressure p^{n+1} is solved from the Poisson equation

$$\nabla^2 p = -[\omega_K\omega_K + \frac{\partial u_i}{\partial x_j}\frac{\partial u_i}{\partial x_j}] \tag{7}$$

which is obtained from the divergence of the momentum equations with solenoidal velocity fields at all times and everywhere. The source terms on the right hand side of (7) are expressed in terms of rectangular cartesian components with summation convention to facilitate computation. The boundary condition for pressure on the non-slip surface is expressed in terms of the solenoidal vorticity field as

$$\frac{\partial p}{\partial\nu} = \bar{\nu}\cdot\nabla p = -\frac{1}{Re}(\nabla\times\bar{\omega})\cdot\bar{\nu} \tag{8}$$

The iterative processes of determining the $\bar{\omega}$, $\bar{q}$ and p at an advanced time step converge rapidly even with a simple discretization algorithm.

The induced potential fields ψ and ϕ in loops (a) and (b) introduce nontrivial instantaneous vorticity. Their contributions on a solid surface through nonzero $\partial\psi/\partial s$ and $\partial\phi/\partial s$ are particularly significant since wave reflection from a solid surface nearly doubles the individual contribution. With, r.m.s. vorticity interpreted as a turbulence measure, this wave propagation process is a powerful mechanism of turbulence production. It is independent of the shear stress in the mean flow, distinct from the convectional turbulence production mechanism, and remains in the inviscid limit.

For illustrative purposes, we carried out the computational simulation of the development of "large disturbances in a uniform shear flow between a stationary plate at $y = 0$ and a moving parallel plate at $y = 1$ with velocity $(1,0,0)$ at $Re = 3000$. The system of equations are discretized with the simple forward time and centered space algorithm using the latest available values in each sweep. The average convective velocity is taken as $\bar{q}^{n+\frac{1}{2}} = \frac{1}{2}(\bar{q}^n + \bar{q}^{n+1})$. The discretized Poisson equations are solved with ADI process with constant acceleration parameters determined from model studies. A coarse grid (15 to 30) x 15 x 15 is used with $\Delta x = 8\Delta y$, $\Delta z = 5\Delta y$ and $\Delta y = 1/14$. The number of mesh points in the x-direction is extended to accommodate the downstream motion of the turbulent spot where necessary. No filtering, smoothing or any other computational artifices have been introduced. All iterative convergence is carried so far that the maximum norm of the changes in $\bar{q}$ for the last iterate is $\lesssim 10^{-3}$. The computer time required to advance (q,p) a time step over the entire field is $\lesssim 2$ sec on IBM 3081, i.e. less than 10^{-3} sec per point. Computations at more refined meshes are being planned. Preliminary results from our coarse mesh computations are reported below.

RESULTS AND DISCUSSION

The development of three types of impulsive disturbances has been computed. They are applied uniformly to the group of mesh points (I,J,K) with $I = 8$, $J = 2,3$ and $K = 7,8,9$ where $J = 1$ $(y = 0)$ is the stationary plate and $K = 8$ the lateral plane of symmetry. The disturbed field is not solenoidal so that the computation starts in the midst of loop (b) or (a) to determine the associated pressure disturbance potential.

Unit impulses of streamwise component vorticity ω_x never grow. Uniform shear flow was reestablished at 50 Δt without any numerical turbulence.

Unit impulses of v-component velocity normal to and away from the stationary plate generates a horseshoe vortex, lifting rapidly from $y = 0$ while being stretched and convected downstream. By 60 Δt, an apparently laminar shear flow is again established with a decaying and diffused horseshoe vortex in the middle. There was no chaotic vortical flows like turbulence in the field.

Unit impulses of u-component velocity generates a complicated three dimensional vortical flow hugging onto the wall $y = 0$, bounded by a high vorticity front propagating slowly in all directions into the neighbouring laminar flow. By 50 Δt, this highly vortical region assumes the well known shape of a turbulent spot over a flat plate as was observed in experiments. Within the vortical region, the flow is chaotic or "turbulent". Outside of the region, the flow is orderly but severely distorted from the undisturbed uniform shear state.

We note the following concerning the developing spot:
(i) The turbulent spot is marked by an irregular high vorticity front advancing into the neighbouring distorted laminar region. A vorticity plateau is present in the center of the spot. Figure 1 illustrates the horizontal sections at $y^+ \simeq 11$ parallel to the plate at 56 Δt, 66 Δt and 86 Δt. The grid points marked by "+" possess local vorticity magnitudes larger than 3. If the cut off of the vorticity magnitude is raised (or lowered), the apparent size of the spot may decrease (or increase) somewhat with the arrow head shape remains essentially the same. If horizontal sections are made at successively larger distances y^+, the general shape of the spot section changes in the manner as was suggested by various experiments.
(ii) The growing "turbulent spot" contains a dominant but diffused horseshoe vortex anchored at the lower plate $y = 0$. The whole structure grows in size and moves downstream at slightly larger than half the moving plate velocity. Figures 2, 3 and 4 illustrate the uv-, v-w and u-w velocity components in various sections at 50 Δt.
(iii) In the plane of symmetry of the initial disturbance and in the midst of the spot, there is a concentrated "sheet" of vertical jet stream directed away from the plate, as is displayed in Figure 3. The jet stream appears to be the induced velocity of the streamwise arms of the horseshoe vortex. There are, however, other details that cannot be so simply rationalized.
(iv) The velocity fluctuation w' in the lateral direction is generally larger than v' within the spot except in the plane of symmetry. As is illustrated in Figure 4 the w' suddenly reaches very large values at the trailing edge of the spot, generating significant trailing "wave packets" that decay gradually further upstream and outside of the spot. Such wave packets are not easily explained by the horseshoe vortex but is a natural consequence of the wave mechanism.
(v) The static pressure variation normal to the plate p(y) in a transverse section across the spot at 56 Δt is illustrated in Figure 5. The pressure valley and the "jet stream" lie in the symmetry plane $K = 8$. The temporal developments of the pressure p(y) and the mean velocity u(y) at a station in the symmetry plane from 56 Δt to 64 Δt are illustrated in Figure 6. Both the pressure and the mean flow velocity are significantly depleted in this region. The pressure valley is the result of the negative definite source terms in the Poisson equation (7).

The restoration of laminar flow conditions for the first two cases provides considerable confidence that "numerical turbulence" is not a significant component in our computed results. The calculated spot development gives global results in agreement with experimental observations. The feasibility of asymptotic computational simulation of the discrete nature of transition and turbulence is demonstrated.

There are important differences between the two cases in which laminar conditions are restored. The magnitudes of vorticity introduced by unit u or v velocity impulses are several times as large as the unit vorticity impulses ω_x. The failure of unit ω_x impulses to produce a turbulent spot is likely due to its small magnitude. We computed also the development of u-velocity impulses of magnitude 0.1 instead of 1. It failed to produce a turbulent spot and uniform shear flow was essentially reestablished at 50 Δt.

The magnitudes of the vortical loops introduced by unit impulses of u and v-component velocities are comparable. A strong horseshoe vortex, which is a dominant flow feature of a well established turbulent spot was created by the v-impulses but it decays when it was lifted away from the stationary wall. By 60 Δt, the laminar flow condition was reestablished. The horseshoe vortex and the turbulent fronts of the associated turbulent region were lifted away from the plate by the positive v-component velocity of the imposed disturbance. The more distant turbulent fronts are less efficient in turbulence production at the wall as they generate weaker or less frequent waves incident on the wall. Deprived of much wall production of turbulence, the vortical region decays as viscous dissipation prevails. The local turbulent region, generated by unit u-velocity impulses was permitted to hug onto the wall so that the wall production mechanism can help to generate and sustain the growing turbulent spot. The relative importance of wave reflection mechanism in the overall turbulence production is quite evident.

To provide a direct test, we calculated the development of impulsive disturbances of streamwise vorticity with $\omega_x = 10$ instead of unity. An asymmetric turbulent spot results. With the imposed u-velocity directed away from the wall on one side and directed toward the wall on the other side, the calculated result shows an extended turbulent region hugging onto the wall on the down drift side and a smaller turbulent finger on the other side, lifting slowly away from the plate. The two regions are connected through a neck in the upstream region with a tendency toward eventual breakup. We are prevented from computing much further to witness the event because of the interference of the side boundaries of our computational domain.

CONCLUDING REMARKS

The wave mechanism of "discrete turbulence" is reviewed against the experimental and mathematical background. Vorticity transport generates pressure waves needed to maintain solenoidal velocity field. The relaxation of these waves as the solution of the initial value problems of the N-S can lead to both smooth and discrete solutions. Smooth solutions correspond to quasi-steady asymptotic states consistent with the Biot and Savart Law. The discrete solution contains local turbulent regions bounded by coalesced wave fronts, propagating into laminar region. The local turbulent region will contain other coalesced wave fronts separating different turbulent states in some form of a multi-layer structure.

This wave mechanism suggests a specific discrete formulation for the computational simulation. We calculated the development of large disturbances in a uniform shear flow at $Re = 3000$. Small disturbances die and laminar flow is restored. Large disturbances generate propagating turbulent spots with global characteristics in good agreement with experimental observations. The computed results support the importance of the wave mechanism of turbulence production expected to be most significant in the proximity of a solid wall where incident waves reflect. This production mechanism is distinct from the conventional one, $-\overline{u_i u_j}\,(\partial U_i/\partial x_j)$, through mean flow shear.

REFERENCES

CANTWELL, B.J. (1981) Organized Motion in Turbulent Flow. Ann. Review Fluid Mech. 13, 457-515. General reference.

CHENG, S.I. (Aug. 1983) Wave and Discrete Nature of Turbulence. VIIth International Congress on Mathematical Physics. Boulder, Colorado, U.S.A.

CHENG, S.I. (Sept. 1983) A New Look on Turbulent Shear Flow. Fourth International Symposium of Turbulent Shear Flow. Karlsruhe, W. Germany.

CHENG, S.I. (1982) Asymptotic Behavior and Best Approximation in Computational Fluid Dynamics. Math. in Comp. Simu. 24, 37-48.

EMMONS, H.W. (1951) The Laminar Turbulent Transitions in a Boundary Layer. Jour. Aero. Sci. 18, 490-498.

HINZE, J.O. (1975) Turbulence, 2nd Ed. McGraw Hill. General reference.

LAMB, H. (1932) Hydrodynamics, 6th Ed. Dover Publications, Art. 1, p. 10; Art. 119, p. 161-162; Art. 152, p. 214-216.

PERRY, A.E., LIM, T.T., CHONG, M.S., and TEH, E.W. (1980) The Fabric of Turbulence. AIAA Paper 80-1348.

RUELLE, D. and TAKENS, F. (1971) On the Nature of Turbulence. Comm. Math. Phys. 20, 167-192.

THEODORSEN, T. (1955) The Structure of Turbulence. in 50 Jahr Grenzschicht Forsung, Ed. H. Götler, W. Tollmien, p. 55. Brunschweig, Veiweg & Sohn.

TOWNSEND, A.A. (1947) Measurements in the Turbulent Wake of a Cylinder. Proc. Roy. Soc. London Ser. A 190, 551-561.

ACKNOWLEDGMENT

This work was performed under the Grant NSFMEA80-10876. The authors wish to thank the National Science Foundation of the United States of America for its interest and support, and the Beijing Institute of Aerodynamics for its cooperation.

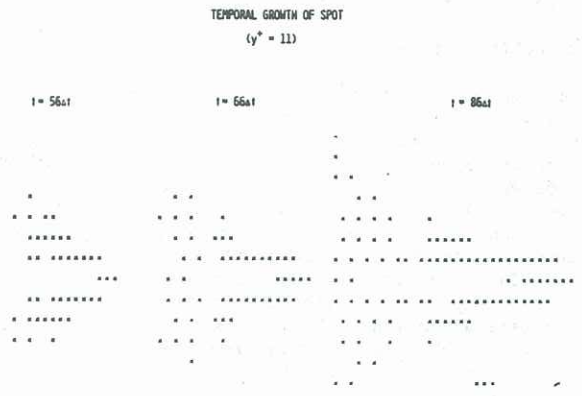

Figure 1

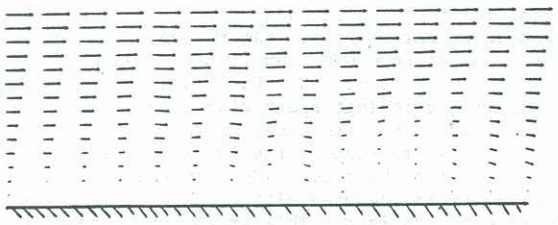

Figure 2 u-v velocity components in plane of symmetry k = 8 at 50 Δt.

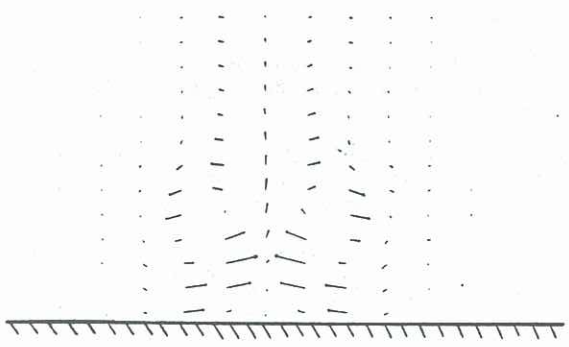

Figure 3 u-w velocity components in a transverse section across the spot at 50 Δt.

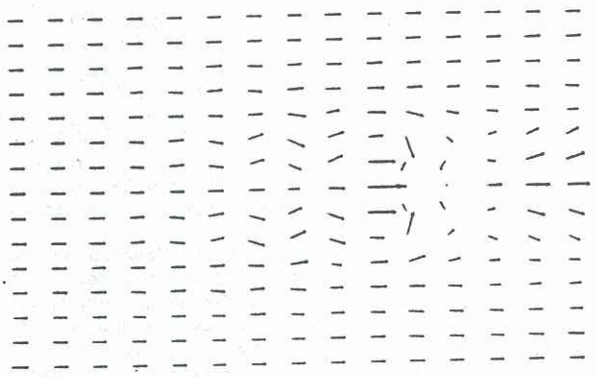

Figure 4 u-w velocity components in horizontal section at $y^+ = 11$ at 50 Δt.

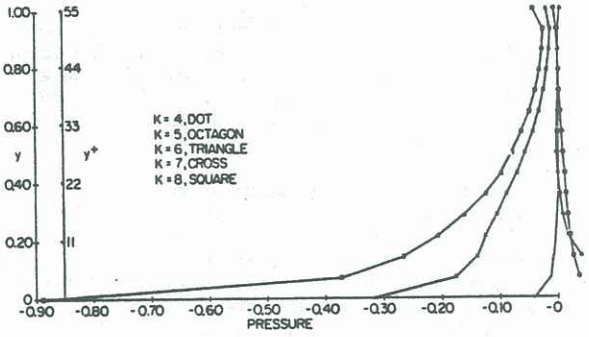

Figure 5 Pressure profile p in a transverse section across the spot at 50 Δt.

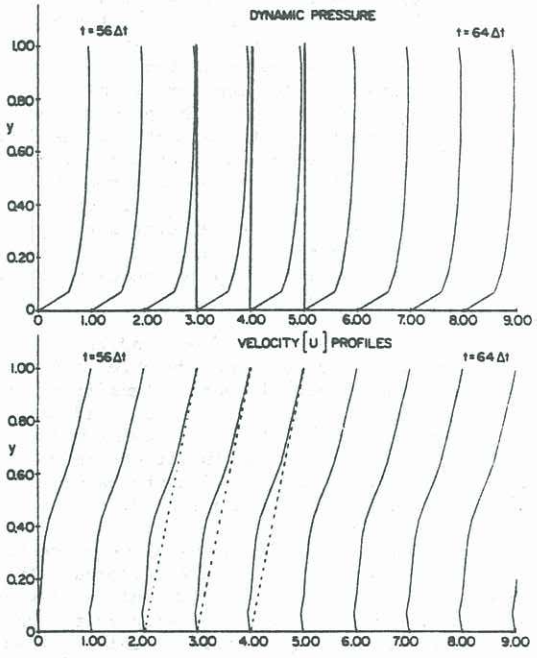

Figure 6 Temporal development of p and u at a point within the spot from 56 Δt to 64 Δt.